Assessment of laminar-turbulent transition modeling methods for the prediction of helicopter rotor performance

François Richez, Alexandre Nazarians, Caroline Lienard
ONERA, The French Aerospace Lab
Meudon, France

ABSTRACT

The influence of the laminar-turbulent transition on helicopter rotor performance in hover and forward flight is investigated by means of URANS simulations. Two different transition modeling approaches are assessed by comparison with available experimental data of the ONERA wind-tunnel scaled 7A rotor. The first one is based on semi-empirical transition criteria and the second one is the Menter-Langtry transport equation model. In hover, Menter-Langtry model slightly improves the prediction of the figure of merit, while transition criteria-based method gives an almost perfect agreement with the experiments. In forward flight, the unsteady motion of the transition obtained with criteria is in fairly good agreement with experimental data deduced from hot film measurements, while Menter-Langtry model shows more unexpected behavior. However, the rotor power predicted by both simulations is very similar. Although transition improves the rotor power prediction in forward flight, the error with respect to the experiments remains still significant.

NOTATION

R	rotor radius, m
c	blade chord, m
b	number of blades
S	rotor disk area, πR^2
σ	rotor solidity, bRc/S
Ω	rotor angular velocity, rad/s
U_∞	freestream velocity, m/s
ρ_∞	freestream fluid density, kg.m^{-3}
a	freestream speed of sound, m/s
M_{tip}	tip Mach number, $(R\Omega)/a$
μ	advance ratio, $U_\infty/(R\Omega)$
T	rotor vertical force in the wind frame, N
Q	rotor torque, N.m
C_T/σ	rotor lift coefficient, $T/[\rho_\infty(R\Omega)^2 S\sigma]$
C_Q/σ	rotor torque coefficient, $Q/[\rho_\infty R(R\Omega)^2 S\sigma]$
P_{ideal}	ideal induced power in hover, $T^{3/2}/\sqrt{2\rho S}$
FM	figure of merit, $P_{ideal}/(Q\Omega)$
ψ	blade azimuth, deg
r	radial coordinate, m
x	chordwise coordinate, m
x_{trans}	chordwise position of transition, m
k	turbulent kinetic energy, m^2/s^{-2}
ω	specific turbulence dissipation rate, s^{-1}
μ_t	turbulent viscosity ratio
γ	intermittency
$Re_{\theta t}$	second variable of the Menter-Langtry model
H_i	boundary-layer shape factor, ratio of displacement and momentum thicknesses

INTRODUCTION

The CFD (Computational Fluid Dynamics) methods have shown a significant expansion in the helicopter community for the recent decades. Despite the high complexity of the flow physics experienced by rotor blades in forward flight, the predictive capabilities of CFD codes in terms of blade structural loads have been recently demonstrated by Ortun *et al.* (Ref. 1) and Yeo *et al.* (Ref. 2). By means of a coupling strategy between a comprehensive analysis code and a CFD code, the authors were able to predict, with an unprecedented accuracy, the loads variations for both high-speed and high-thrust forward flights. This has been made possible through a meticulous attention to each detail of the flow that is necessary to capture the whole rotor flow physics: conservation of the tip vortex wake, accurate spatial resolution of the viscous boundary layer, accurate turbulence model for flow separation, shock-capturing scheme, blade deformation, and suitable time resolution.

However, another element of the flow physics that can be of main interest in helicopter rotor flow and that is still too often neglected in numerical simulations is the laminar-to-turbulent transition process of the boundary layer. In hover, experimental investigations showed that large laminar regions appear on the blade, especially on the lower side (Ref. 3). Not taken into account these laminar flow regions in numerical simulations can lead to a significant overestimation of the power consumption of the rotor (Refs.

Presented at the 43rd European Rotorcraft Forum, Milan, Italy, September 12-15, 2017.

4-5). In forward flight, the unsteady transition process is expected to be more complex and is undeniably more challenging for both experimental measurement and numerical simulation. Thus, the mechanisms of laminar-to-turbulent transition on rotor blades in forward flight and their consequences on the rotor performance are still unknown. Hot films measurements on the 7A wind-tunnel scaled rotor provided some helpful data on the transition location for a forward flight condition (Ref. 6). Beaumier and Houdeville first attempted to predict transition for this flight case by means of a coupling method between potential and boundary layer codes (Ref. 7). In the framework of the RANS (Reynolds-Averaged Navier-Stokes) approach which is now largely accepted, transition criteria have been developed in order to correct the turbulence model and allow the RANS simulation to impose laminar flow regions where required (Ref. 8). With this approach, several transition processes such as Tollmien-Schlichting instabilities, crossfow instabilities, laminar separation bubble or bypass mechanism can be taken into account at the same time in a single simulation. Recent works of Heister takes advantages of this criteria approach to identify the different transition mechanisms involved on the rotor blades in forward flights (Ref. 9). However, this method suffers from several drawbacks: it can be very complex to implement. It requires to compute integral boundary layer quantities which is not numerically robust. It assumes that the flow is following the grid lines, a condition which is not always satisfied for rotor blades in forward flight.

In 2004, a new transition modelling approach came out, and has been since then increasingly popular in the CFD community. This model was first partially published by Menter and Langtry (Refs. 10-11) and was finally made public by its authors in its complete formulation in 2009 (Ref. 12). It is based on transport equations of two new variables (γ and $Re_{\theta t}$) which made this method easy to implement, numerically robust, and applicable to every kinds of flow configurations whatever the grid topology is. Furthermore it offers a simplified interface for the user. On the other hand, the Langtry correlation which is the base of the $\gamma - Re_{\theta t}$ model has shown some limitations for some flow conditions, such as adverse pressure gradient, relaminarization or turbulence contamination (Ref. 13).

The objective of the present paper is to assess the capabilities of these two transition modeling approaches, criteria-based method and $\gamma - Re_{\theta t}$ transport equation model, for helicopter rotor in hover and forward flights. First, the ONERA 7A rotor in hover is considered. The evolution of the predicted transition location with respect to the rotor thrust and its impact on the rotor performance are analyzed. Then, a configuration of 7A rotor in forward flight is considered. In this case, a loose coupling strategy between *elsA* CFD code (Ref. 14) and HOST comprehensive analysis tool (Ref. 15) is used to compute the rotor control angles and blade deformation that enable to reach the desired flight condition. The two different transition modeling methods are then assessed for this forward flight condition.

TRANSITION MODELING

Two different methods to take into account transition in RANS simulation are used in this paper.

The first one is based on transition criteria. These criteria rely on boundary layer integral parameters and sometimes on the boundary layer history. Two kinds of criteria can be used. The first one, called AHD, has been proposed by Arnal *et al.* in Ref. 8 and its complete formulation can be found in Ref. 13. This criterion is based on stability calculation of similar boundary layer velocity profiles. It provides the expected transition point when the transition process is due to the growth of Tollmien-Schlichting instable waves. This transition scenario, often referred-to as “natural transition”, is the most usual one in external flow configurations. It is valid for a Mach number up to 1.6 and for a turbulence level up to 1%.

Sometimes, another mechanism based on crossflow (CF) instability can lead to the transition of laminar boundary layer before Tollmien-Schlichting waves become unstable. This instability mechanism is related to the intensity of the spanwise flow inside the boundary layer. In order to take into account this transition scenario, referred to as CF transition, a second criterion, called C1, has been proposed by Arnal *et al.* in Ref. 8.

Both AHD and C1 criteria can be taken into account simultaneously. The first criterion that is reached determines the transition position in the simulation. This position is used to compute an intermittency field, defined on the wall, such as $\gamma = 0$ in laminar regions and $\gamma = 1$ in turbulent regions. Then, γ is applied to all the points of the computational domain, by following the normal to the nearest wall and weighting the eddy viscosity such that $\mu_t^{eff} = \gamma \mu_t$. When combined to a $k - \omega$ SST turbulence model (Ref. 16), this approach allows to put to zero the k production, which is proportional to μ_t^{eff}, in the laminar regions.

The second transition method, proposed by Menter and Langtry (Ref. 10), is based on transport equations of two new quantities, γ and $Re_{\theta t}$. The first one corresponds to an intermittency field. Contrary to the previous criteria approach, γ is not here a two-dimensional field defined at the wall but three-dimensional field defined in the whole fluid domain. It is driven by a classical transport equation, with time-derivative, convection, production, destruction and diffusion terms. This γ field is then used to weight the production term in the k transport equation of the SST turbulence model. The second quantity, $Re_{\theta t}$, is used to provide locally, inside the boundary layer, the empirical correlation that decides whether the flow is laminar or turbulent and drives accordingly the production of γ.

Hover

The rotor used for hover condition is the 7A wind-tunnel scaled four-bladed rotor. Its radius is $R = 2.1$ m and its chord $c = 0.14$ m. The blade rotation velocity is set in order to reach a tip Mach number $M_{tip} = 0.62$. The blade is

aerodynamically twisted with a constant rate of -8.3 deg/R. Two airfoils are used, OA213 airfoil of 13% relative thickness in the innermost part of the blade ($r/R \leq 0.75$) and OA209 airfoil of 9% relative thickness in the tip region ($r/R \geq 0.9$).

Taking advantage of the rotational symmetry of the problem, the computational domain is reduced to a quarter cylinder around one single blade. It extends over $6R$ in the radial direction and $12R$ in the vertical direction. Periodicity conditions are imposed on the lateral boundaries. Specific hover conditions derived from momentum theory are imposed on the upper, lower and external boundaries of the computational domain. This avoids undesirable blockage effects that could give rise to massive flow recirculation above the rotor. A Chimera strategy is adopted. The blade grid is composed of 3 million points and the Cartesian backward grid is composed of 9 million points (Fig. 1).

The simulations are performed with the *elsA* solver which discretizes the Reynolds-Averaged Navier-Stokes (RANS) equations with a finite-volume approach on structured multiblock mesh (Ref. 14). For all the simulations, the $k-\omega$ SST turbulence model proposed by Menter is used (Ref. 16). For the transition simulations, the turbulence level is set to $Tu = 0.5\%$. The simulations are performed at four different collective pitch angles in order to sweep a large range of rotor thrust coefficient between $C_T/\sigma = 0.03$ and $C_T/\sigma = 0.11$. Simulations are first performed in fully turbulent mode, i.e. the turbulent model numerically switches from laminar to turbulent flows close to the leading edge. Then, simulations are run with transition criteria-based approach and Menter-Langtry model. With transition criteria-based approach, only AHD criterion is applied since no crossflow instability is expected.

The same numerical schemes are used for all the simulations. The convective flux is discretized with a second-order Jameson scheme, while a second order centered scheme is used for the viscous flux. For the hover cases, the RANS equations are solved in the rotating frame where the solution is expected to be steady. Thus, a simple first-order implicit backward-Euler scheme with a local time stepping approach is chosen to discretize the time derivative and converge quickly to the steady state.

The evolution of the figure of merit FM as a function of the rotor thrust coefficient is shown in Fig. 2. Table 1 provides the numerical values of FM for each thrust coefficients and, in brackets, the relative error with respect to the experimental data. The transition clearly improves the prediction of the rotor performance. The fully turbulent simulations significantly under-predicts the FM all along the rotor thrust range with a relative error between 5 and 7%. When the Menter-Langtry model is used, the relative error is slightly reduced to reach 4%. The AHD criterion allows to predict the figure of merit with an error less than 1% for the whole rotor thrust range.

In order to explain the origin of this performance gain, the transition position along the blade is shown in Fig. 3 for both criteria-based and Menter-Langtry model approaches at $C_T/\sigma = 0.1$. With Menter-Langtry model the transition position is not clearly defined since the intermittency γ is a three-dimensional field that fulfills $\gamma = 0$ at the wall. Thus, it has been decided to define the transition position from a criteria based on the boundary layer shape factor Hi. Since the shape factor is expected to be 2.6 in laminar boundary layer and 1.4 in turbulent boundary layer, the critical value $Hi = 2$ is chosen as an adequate indicator of the transition position. This iso-value of Hi is depicted in black line in Fig. 3. On the upper side of the blade, Fig. 3.a shows that the transition position predicted by the AHD criterion is almost constant along the blade span and located around x/c=10%. Let us remark that a second line corresponding to $Hi = 2$ also appears in the trailing edge region. This is not related to transition, but to the fact that the turbulent boundary layer is not far from separating from the wall which leads to an increase of Hi. On the lower side of the blade (Fig. 3.b), the transition is located very close to the trailing edge and with very small variations with respect to the radial position r/R.

With Menter-Langtry model (Fig. 3.c and d), the transition point significantly changes with respect to the radial position for both the upper and lower sides. For $0.5 \leq r/R \leq 0.85$, the transition position on the upper side (Fig. 3.c) is very similar to what was observed with AHD criterion (Fig. 3.a): The boundary layer gets turbulent around $x/c = 10\%$. For $0.3 \leq r/R \leq 0.6$, the transition on the lower side of the blade remains almost laminar until the trailing edge with Menter-Langtry model (Fig. 3.d), exactly as AHD does (Fig. 3.b). However, in the tip region ($r/R \geq 0.8$) the transition with Menter-Langtry moves to leading edge on both sides of the blades. A particular attention to the flow field shows that this is due to the impact of the turbulent tip vortex emitting by the preceding blade. The tip vortex thus convects high eddy viscosity values into the boundary layer that makes the flow turbulent. With the criteria approach, no similar kind of by-pass transition mechanisms is taken into account, so that the flow is computed as laminar by the criteria in the region where tip vortex interaction occurs. The same effect is observed at the blade root in Fig. 3.b and Fig. 3.d. The Menter-Langtry model shows a region of turbulent flow because of the impact of the root vortex emitted by the preceding blade.

On the innermost part of the blade, for $0.25 \leq r/R \leq 0.5$, the two transition approaches also show some differences on the upper side. The Menter-Langtry predicts that the transition moves back to reach mid-chord at $r/R = 0.32$ (Fig. 3.c) while it remains close the leading edge all along the radial direction with the AHD criterion (Fig. 3.a). The transition point is not expected to move downstream in this blade region where the angle of attack is increased because of the blade twist. Nevertheless, the transition position in the innermost part of the blade should not affect significantly the overall performance of the rotor, since the profile power is mainly driven by the profile drag on the blade tip region.

Thus, it can be concluded that the gain in FM is higher with criteria-based approach, as shown in Table 1, because

the flow remains laminar on the whole lower side of the blade tip (Fig. 3.b), while Menter-Langtry model predicts a fully turbulent flow (Fig. 3.d) due to the impact of the tip vortex. For the considered configuration, no experimental measurement that could confirm the effect of the tip vortex on the transition location has been conducted. In the literature, most of the experimental investigations of transition on helicopter rotor in hover show a large laminar region on the lower side of the blade (Refs. 17-19). In Ref. 19, a small turbulent pocket, that could be related to tip vortex interaction, only appears at very low thrust coefficients ($C_T/\sigma \leq 0.045$). For higher thrust where the figure of merit is close to its maximum, no tip vortex-induced transition has been experimentally observed. In consequence, it is reasonable to think that the tip vortex should not trigger the transition on the lower side of the blade tip in hover condition. This may explain why AHD criterion gives better results than Menter-Langtry model for this hover condition. However, further experimental investigations will be necessary to draw clear and definitive conclusions.

FORWARD FLIGHT

The isolated 7A rotor in forward flight condition is considered in this section. The advance ratio is $\mu = 0.3$ and the thrust coefficient $C_T/\sigma = 0.063$. An *elsA*/HOST coupling simulation has been first performed with a fully turbulent approach in order to the reach the aero-mechanical equilibrium of this flight condition in terms of rotor control angles and blade deformation. At each coupling iteration, the CFD loads computed by *elsA* is provided to the comprehensive code HOST which, in return, computes a new aero-mechanical equilibrium of the blades and provides the new kinematics and deformation to *elsA* for the next CFD simulation. After several coupling iterations, the rotor control angles are stabilized and the simulation is considered as converged. Transition simulations, with both criteria and Menter-Langry approaches, have then been performed, remaining unchanged the blade motion and deformation compared to the fully turbulent simulation.

For these forward flight conditions, a second-order implicit time-discretization method with lower-upper (LU) factorization and Newton iterations is used. The azimuthal time step is $\Delta\psi = 1$ deg and the maximum number of sub-iterations of the Newton process is fixed to 30 for all the simulations.

Influence of the transition criterion

When applying transition criteria, some precautions have been taken to avoid any robustness issues of the method. Indeed, for a helicopter rotor in forward flight condition, reverse flow appears on a region of the retreating blade side. Criteria can easily fail to correctly compute transition point when the flow is reverse. Thus, this region is imposed as turbulent. For similar reasons of robustness, the flow is also imposed as turbulent in thin region of span equal to half-chord length at the blade tip.

Two simulations with transition criteria approach have been performed, a first one where only AHD criterion is applied and a second one with both AHD and C1 criteria. This allows to easily detect where crossflow instability transition is found by C1 criterion.

The transition chordwise position computed with AHD criteria is shown in Fig. 4. This position is simply defined at the wall position where the intermittency gets from 0 to 1. On the upper side (Fig. 4.a) transition position does not significantly vary during the blade rotation, except close to the root. On the tip region, it moves downstream on the advancing blade where it reaches values between 20 and 30% of chord, while it moves to the leading edge on the retreating blade to reach $x_{trans}/c \leq 0.1$. Close to the reverse flow region of the retreating blade, the transition position moves back to the trailing edge in a small region located at $r/R \leq 0.6$ and $240 \leq \psi \leq 330$. This delay of the transition is due to a strong decrease of the local Reynolds number induced by a low local relative velocity.

On the lower side of the blade (Fig. 4.b), transition position moves significantly during the blade rotation. On the advancing blade side, the transition station is almost at the leading edge for all radial and azimuthal positions. Then, on the retreating blade side, it moves back to a station located between 70% and 90% of chord. This follows the expected behavior of the transition since the local angles of attack are decreased on the sections of the advancing blade and increased on the sections of the retreating blade.

A similar simulation has then been performed with both AHD and C1 criteria in order to identify regions where transition can be lead by crossflow instability mechanisms. The transition positions thus obtained is shown in Fig. 5. By comparing Fig. 5 and Fig. 4, regions of crossflow transition have been detected. These are pointed out in dashed white line and denoted by CF in Fig. 5. On the upper side, CF transition only occurs on a small region located in the innermost part of the retreating blade. In this region, the AHD criterion indeed predicts a transition delay due to the low local Reynolds number, as pointed out previously. On the other hand, the spanwise flow is strong on the retreating blade. Finally, C1 criterion is thus reached before AHD and leads to transition at the leading edge.

On the lower side of the blade, the discrepancy between the AHD (Fig. 4.b) and AHD+C1 (Fig. 5.b) results is stronger. Indeed, CF transition is detected by C1 criteria on a large part of the retreating blade between the azimuthal positions $\psi = 210$ deg and $\psi = 340$ deg. In this portion of the rotor disk, AHD criteria predicted a large laminar flow region. But, finally, the spanwise flow is seen as strong enough by C1 criterion to trigger the transition at an upstream position.

In order to confirm the existence of CF transition process, the transition positions predicted by the two simulations have been compared to available experimental data. During the wind-tunnel test of the 7A rotor, some hot films measurements have been used to identify the regions of

laminar and turbulent flows on a section located at $r/R = 0.9$ (Ref. 6). This data are compared to the numerical results in Fig. 6. The azimuthal evolution of these laminar and turbulent regions is shown respectively in blue and pink. The transition is thus expected to occur in the experiment in between these colored areas. The transition positions obtained with AHD and AHD+C1 are also shown in Fig. 6. On the upper side of the blade, the two simulations give the same transition since no CF transition is involved at the tip section. The numerical prediction of the transition gives satisfactory results with respect to the experimental data. The transition point smoothly moves from 10% of chord at $\psi = 0$ deg to a station located between 25 and 35% of chord at $\psi = 60$ deg. Then it moves back to the leading edge region on the retreating blade side. Experiment and simulation do not perfectly agree on the time phase where this occurs. This happens between 240 and 270 of azimuth in the experiment and at $\psi = 180$ deg in the numerical simulation.

On the lower side of the blade, AHD criterion provides results in fairly good agreement with the experiment. C1 criterion gives an earlier transition on the retreating blade between 210 and 330 deg, which does not seem to be confirmed by the experiment. Indeed, the hot films measurements tend to show that the transition reaches the trailing edge region for $270 \leq \psi \leq 300$, as predicted by AHD.

The effect of the transition on the prediction of the rotor torque coefficient is shown in Table 2. The fully turbulent simulation significantly overestimates C_Q by 20%. When transition is taken in account, this error is reduced to 14% with AHD criterion and 15% when both AHD and C1criteria are applied. In both cases, the transition modeling improves the prediction of rotor performance but not enough to get satisfactory results.

Comparison between criteria-based and Menter-Langtry approaches

The same condition of rotor in forward flight has been computed with the Menter-Langtry model. In the previous section dedicated to AHD and C1 criteria, the transition position was defined as the wall position where the intermittency moves from 0 to 1. However, the extraction of a transition position based on quantities defined on the blade surface is not as obvious with the Menter-Langtry model as for the criteria-based approach. Indeed, the intermittency variable of the Menter-Langtry model is a three-dimensional field that takes zero value at the wall in both laminar and turbulent regions. Thus, a different way of defining transition position has to be used. As we did previously for the hover flight condition, the transition position is here defined by the first wall position where the shape factor gets lower than a critical value set to $Hi = 2$. In order to have comparable results between criteria approach and Menter-Langtry model, the same method to compute the transition position have been applied for both simulations. The results thus obtained are shown in Fig. 7 for AHD and in Fig. 8 for Menter-Langtry. Because the method to define the transition position is not flawless, the results have been checked *a posteriori*, and the erroneous transition positions have been removed from the figures. Neglecting this erroneous regions, one can see that, for the same AHD results, the transition position defined with H_i in Fig. 7 is very close the one of Fig. 4 where the transition position is based on the intermittency.

This check being done, the transition positions can be compared between AHD and Menter-Langtry. On the upper side of the blade (Fig. 7.a and Fig. 8.a), the results are roughly similar. In both cases, the transition is located in the first 30% of chord. However, the region close to the blade tip where the most downstream transition is observed defers between the two approaches. While AHD criteria gives a transition delay on the advancing blade for $60 \leq \psi \leq 120$, this occurs later, for $150 \leq \psi \leq 270$ with Menter-Langtry model.

On the lower side, the differences between the two approaches are more significant. While transition with AHD remains at the leading edge in the whole advancing blade side (Fig. 7.b), with Menter-Langtry, it quickly moves to mid-chord to finally go back to the leading edge between $\psi = 60$ deg and $\psi = 120$ deg (Fig. 8.b). The origin of this quick variation of the transition has not yet been identified. On the lower side, the transition with Menter-Langtry follows roughly the same trend as AHD. For $\psi \geq 180$ deg, the transition moves toward the trailing edge. However, it barely reaches 50% of chord with Menter-Langtry while it goes to the trailing edge with AHD criterion.

Fig. 9 compares the azimuthal evolution of the transition point at $r/R = 0.9$ between AHD, Menter-Langtry and the experimental data provided by the hot film measurements. On the upper side of the blade, both simulations provide similar results in satisfactory agreement with experiments. On the lower side, the unexplained behavior of the transition point of Menter-Langtry model around $\psi = 60$ deg does not seem to follow any experimental trend. On the retreating blade side, the large motion of the transition point from the leading to the trailing is significantly underestimated by Menter-Langtry while AHD criterion gives more satisfactory results.

Finally, the prediction of the torque coefficient provided by Menter-Langtry model is compared to the other results in Table 2. Despite the significant discrepancy between AHD and Menter-Langtry in terms of transition position, the torque coefficient predicted by both approaches is finally the same. The decrease of power due to laminar regions allows to decrease the relative error with respect to the experiments. However, this error, of 14%, is still too high to have satisfactory predictability capabilities.

CONCLUSION

The influence of laminar-turbulent transition on helicopter rotor performance has been numerically investigated. Two different transition modeling approaches

have been considered. The first one is based on semi-empirical criteria that are defined with respect to the history of boundary layer quantities. The second one, proposed by Menter and Langtry, is based on transport equations. The criteria approach allows to take into account, in the same simulation, several transition processes. AHD criterion is applied for natural transition while C1 criterion provides the position of the transition due to crossflow instability. For Menter-Langtry approach, only the original model that predicts natural or by-pass transition has been used. The two methods have been assessed for isolated rotor in hover and forward flights. In hover, both transition approaches improve the figure of merit prediction, with a higher benefit to the criteria approach which gives an error less than 1%.

For the forward flight condition, the prediction of the transition position has been compared to available experimental data. It shows that AHD criterion provides satisfactory results. When crossflow transition is taken into account by means of C1 criterion, the agreement with experiment is less good. Menter-Langtry model provides very different transition positions that deviate further from the experiments. In any case, both technics improves the rotor power prediction, but the relative error with respect to the experiment is still higher than 10%. Some effort has thus to be put in order to identify other mechanisms that has to be taken into account in the simulation to improve the capability of CFD to predict helicopter rotor performance.

REFERENCES

[1] Ortun, B., Potsdam, M., Yeo, H., "Rotor Loads Prediction on the ONERA 7A using Fluid/Structure Coupling", 72nd AHS Annual Forum, West Palm Beach, Florida USA, May 2016.

[2] Yeo, H., Potsdam, M., Ortun, B. Van Truong, K., "High-Fidelity Structural Loads Analysis of the ONERA 7A Rotor", 42nd European Rotorcraft Forum, Lille, France, September 5-9, 2016.

[3] Rohardt, C. H.,"Flow Visualization on a Helicopter Rotor in Hover Using Acenaphthen", 13th European Rotorcraft Forum, Arles, France, 1987.

[4] Beaumier, P., Chelli, E. and Pahlke, K., "Navier-Stokes Prediction of Helicopter Rotor Performance in Hover including Aero-elastic Effects", American Helicopter Society 56th Annual Forum, Virginia, 2000.

[5] Heister, C., "Semi-/empirical transition prediction and application to an isolated rotor in hover", Int. J. Engineering Systems Modelling and Simulation, Vol. 4, No. 1/2, 2012.

[6] Sémézis, Y. and Beaumier, P., "Détermination de l'état de la couche limite sur des sections de pale d'hélicoptère à l'aide de films chauds", 31ème Colloque d'Aérodynamique Appliquée, Paris, France, mars 1995.

[7] Beaumier, P. and Houdeville, R., "3D laminar-turbulent boundary layer calculations on helicopter rotors in forward flight: application to drag prediction, 21st European Rotorcraft Forum, Saint-Petersburg, Russia, September 1995.

[8] Arnal, A., Habiballah, M. and Coustols, E., "Laminar Instability Theory and Transition Criteria in Two and Three Dimensional Flow", La Recherche Aérospatiale, No. 1984-2, 1984.

[9] Heister, C., "Approximate Transition Prediction for the ONERA 7AD Rotor in Forward Flight using a Structured and Unstructured U/RANS solver", 72nd American Helicopter Society Forum, West Palm Beach, Florida, May 2016.

[10] Menter, F. R., Langtry, R. B., Likki, S. R., Suzen, Y. B., Huang, P. G. and Völker, S., "A correlation-based transition model using local variables-Part I: Model formulation", J. Turbomach. 2004, Vol. 128, No. 3, pp. 413-422, doi: 10.1115/1.2184352

[11] Langtry, R. B., Menter, F. R., Likki, S. R., Suzen, Y. B., Huang, P. G. and Völker, S., "A Correlation-Based Transition Model Using Local Variables-Part II: Test Cases and Industrial Applications", J. Turbomach., 2004, Vol. 128, No. 3, pp. 423-434, doi: 10.1115/1.2184353

[12] Langtry, R. B. and Menter, F. R., "Correlation-Based Transition Modeling for Unstructured Parallelized Computational Fluid Dynamics Codes", AIAA Journal, 2009, Vol. 47, No. 12, pp. 2894-2906.

[13] Perraud, J., Deniau, H. and Casalis G., "Overview of transition prediction tools in the *elsA* software", ECCOMAS conference, Barcelona, Spain, July 2014.

[14] Cambier, L., Heib, S. and Plot, S., "The ONERA *elsA* CFD software: input from research and feedback from industry", Mechanics & Industry, 14 (3), pp. 159-174, 2013.

[15] Benoit, B., "HOST A General Helicopter Simulation Tool for Germany and France", 56th Annual Forum of the Helicopter Society, Virginia Beach, VA, USA, 2000.

[16] Menter, F. R., "Two-equation eddy-viscosity transport turbulence model for engineering applications", AIAA Journal, 1994, Vol. 32, pp. 2066-2072.

[17] Richter, K. and Schulein, E., "Boundary-layer transition measurements on hovering helicopter rotors by infrared thermography," Experimental in Fluids, 2014.

[18] Richter, K., Schülein, E., Ewers, B., Raddatz, J. and Klein, A., "Boundary Layer Transition Characteristics of a Full-Scale Helicopter Rotor in Hover", Proceedings of the 72nd American Helicopter Society Forum, West Palm Beach, Florida, May 2016.

[19] Overmeyer, A. D. and Martin, P. B., "Measured Boundary Layer Transition and Rotor Hover Performance at Model Scale", Proceedings of the 55th AIAA Aerospace Science Meeting, Grapeville, Texas, January 2017.

Table 1. Comparison of the figure of merit *FM* between numerical simulations and experiments. The relative error with respect to experiment is indicated in brackets.

C_T/σ	Exp.	Fully Turbulent	Menter-Langtry	AHD Criterion
0.035	0.475	0.459 (-3.4%)	0.478 (-0.6%)	0.492 (+3.6%)
0.055	0.640	0.597 (-6.7%)	0.615 (-3.9%)	0.635 (-0.8%)
0.075	0.717	0.673 (-6.1%)	0.687 (-4.2%)	0.722 (+0.7%)
0.1	0.736	0.700 (-4.9%)	0.710 (-3.5%)	0.738 (+0.3%)
0.112	0.733	0.695 (-5.2%)	0.705 (-3.8%)	0.732 (-0.1%)

Table 2. Rotor torque coefficient C_Q obtained in forward flight.

	Exp.	Fully turbulent	AHD criterion	AHD+C1 criteria	Menter-Langtry
C_Q	0.0037	0.00445 (+20%)	0.00424 (+14%)	0.00426 (+15%)	0.0422 (+14%)

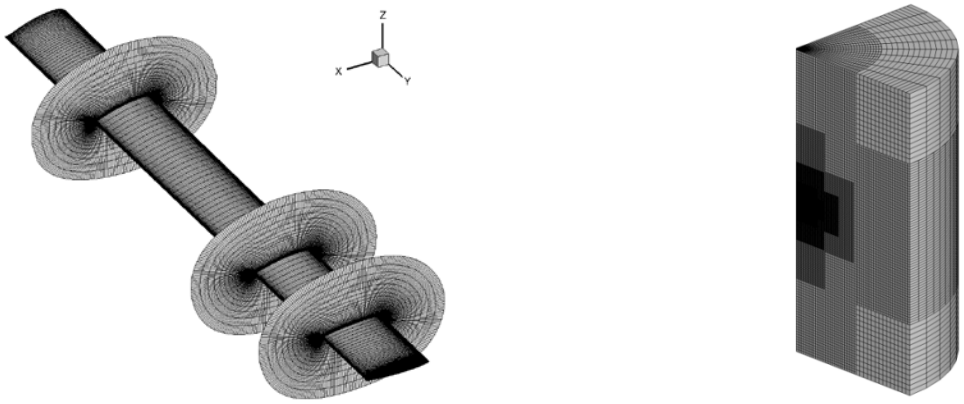

a) Blade curvilinear grid *b) Cartesian background grid*

Fig. 1. View of the blade grid (a) and Cartesian background grid (b) for the hover simulations.

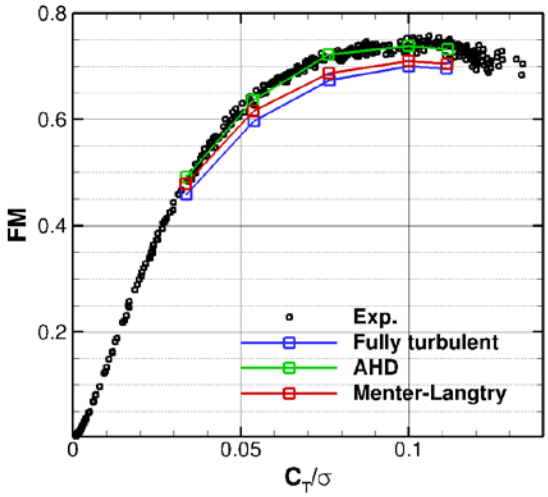

Fig. 2. Figure of merit FM as a function of the rotor thrust coefficient C_T/σ.

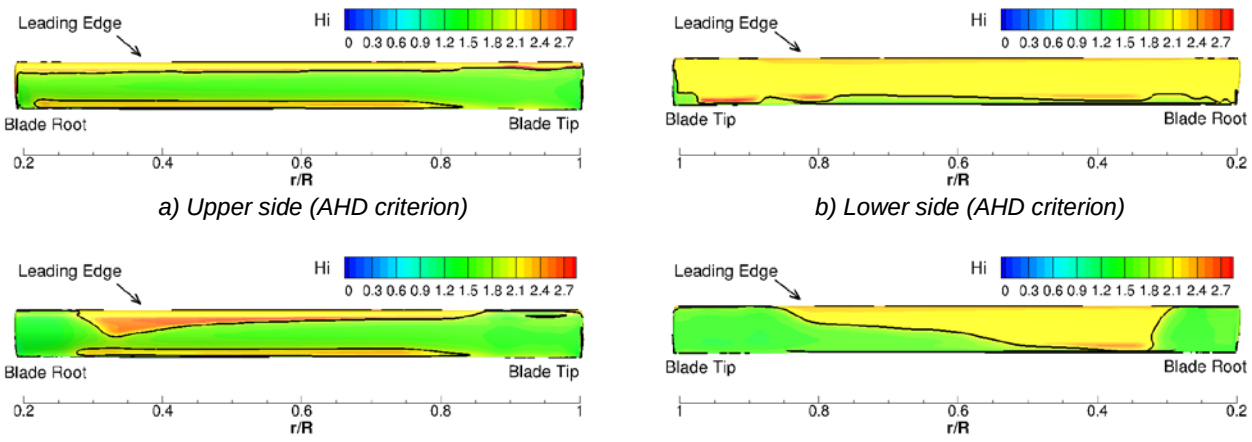

a) Upper side (AHD criterion) *b) Lower side (AHD criterion)*

c) Upper side (Menter-Langtry model) *d) Lower side (Menter-Langtry model)*

Fig. 3. Boundary layer shape factor Hi obtained in hover at $C_T/\sigma = 0.1$ (The iso-value $Hi = 2$ is indicated in black line as an estimation of the transition location).

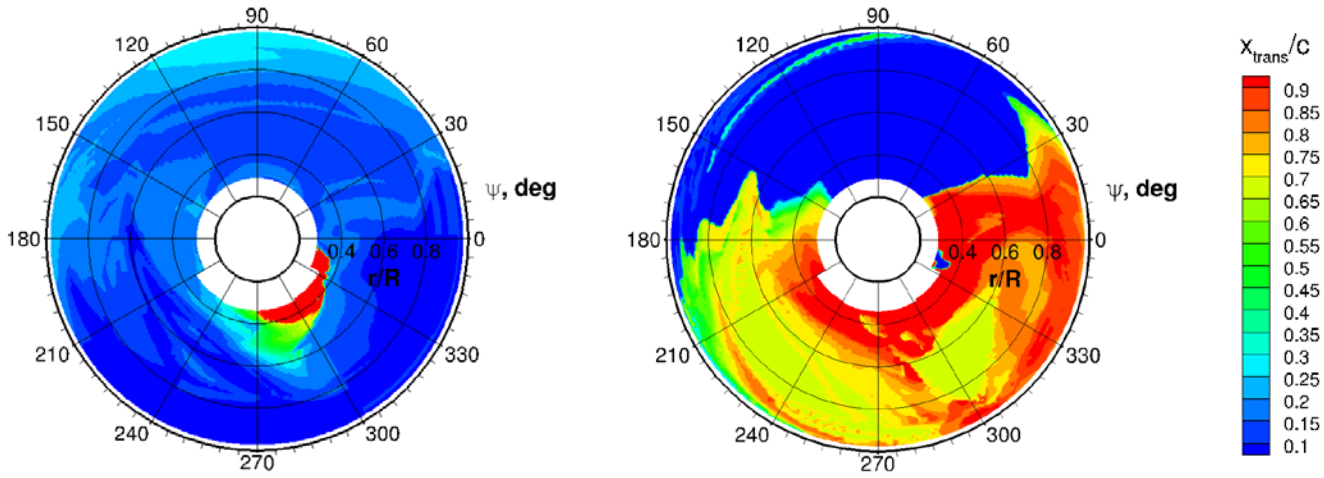

a) Upper side (AHD criterion) *b) Lower side (AHD criterion)*

Fig. 4. Rotormap of the chordwise positions of transition on the upper and lower sides of the blade, obtained with AHD criterion the forward flight case.

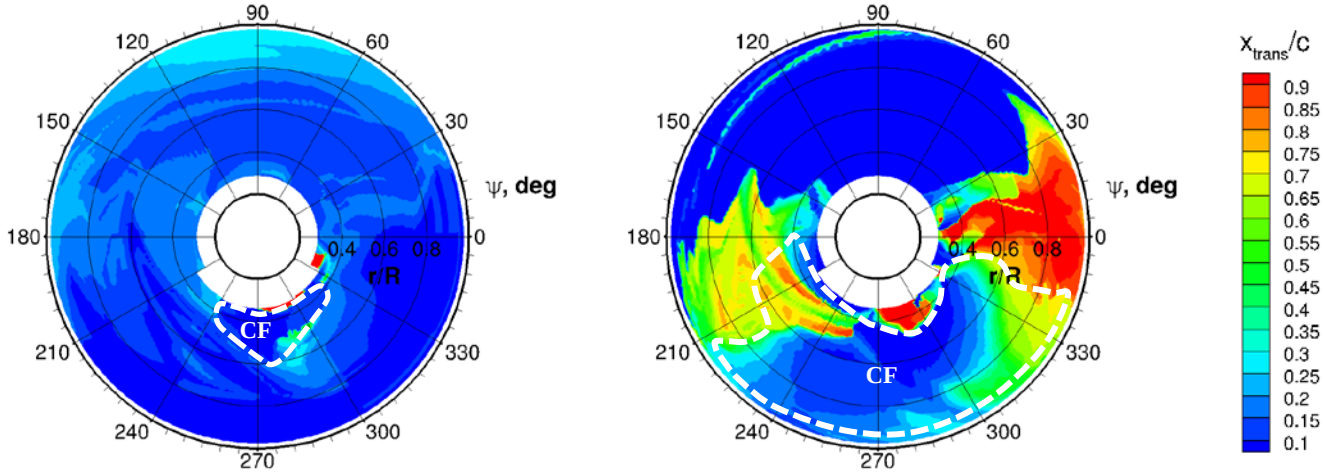

a) Upper side (AHD+C1 criteria) *b) Lower side (AHD+C1 criteria)*

Fig. 5. Rotormap of the chordwise positions of transition on the upper and lower sides of the blade, obtained with AHD anc C1 criteria in the forward flight case.

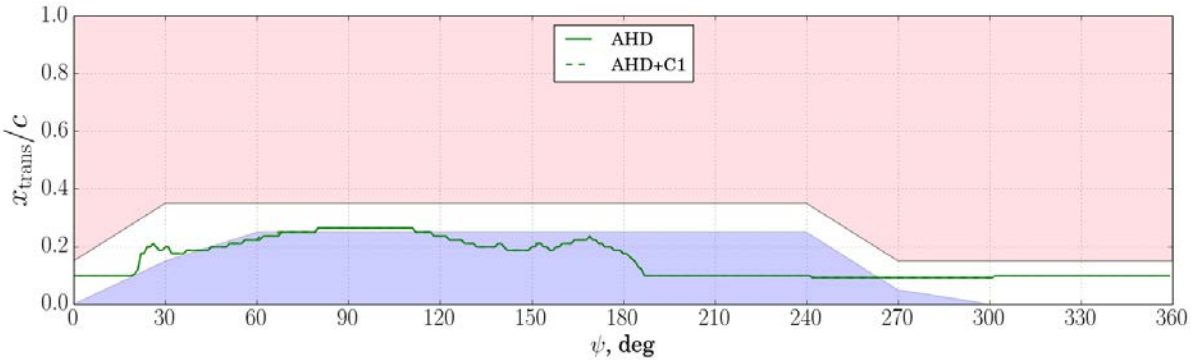

a) Upper side

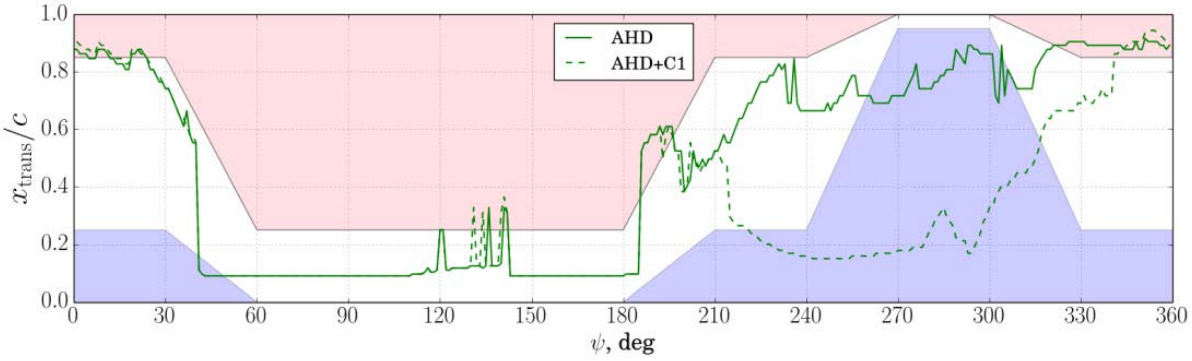

a) Lower side

Fig. 6. Azimuthal evolution of the transition location at section r/R=0.9 on the upper side (a) and lower side (b) of the rotor blade in forward flight condition: AHD criterion (solid green line), AHD+C1 criteria (dashed green line). Blue (respectively pink) region indicates laminar (respectively turbulent) region in the experiment.

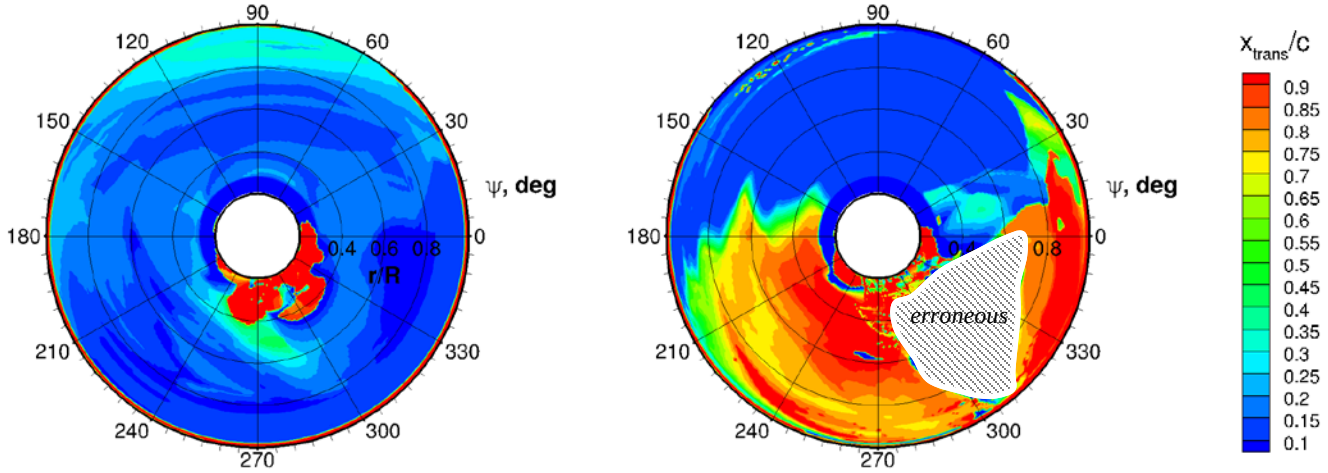

a) Upper side (AHD criterion) *b) Lower side (AHD criterion)*

Fig. 7. Rotormap of the transition position deduced from the shape factor H_i obtained with the AHD criterion applied to the forward flight condition.

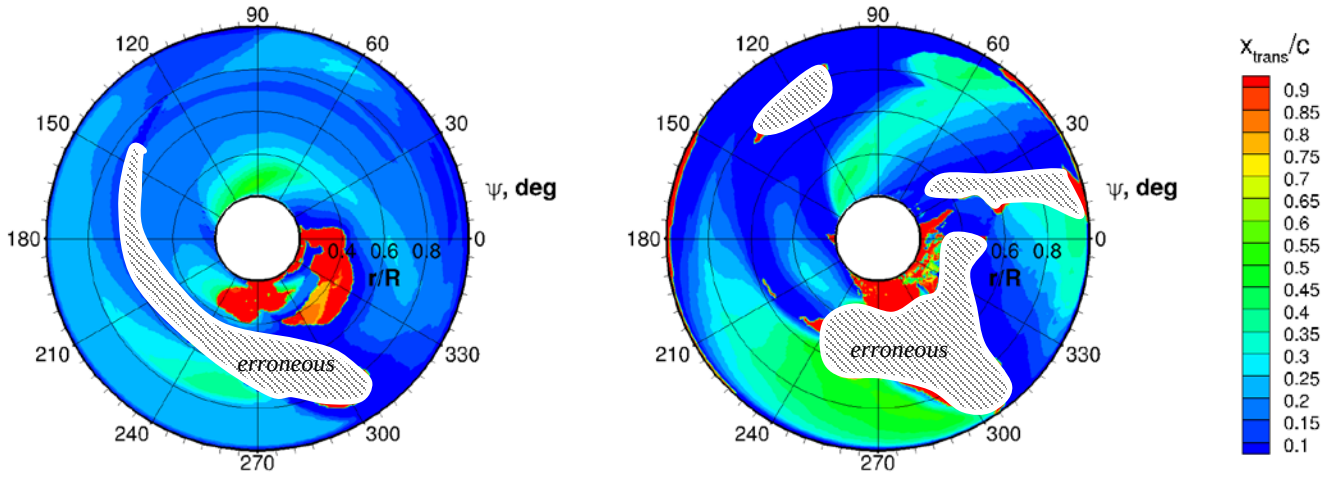

a) Upper side (Menter-Langtry) *b) Lower side (Menter-Langtry)*

Fig. 8. Rotormap of the transition position deduced from the shape factor H_i obtained with the Menter-Langtry model applied to the forward flight condition.

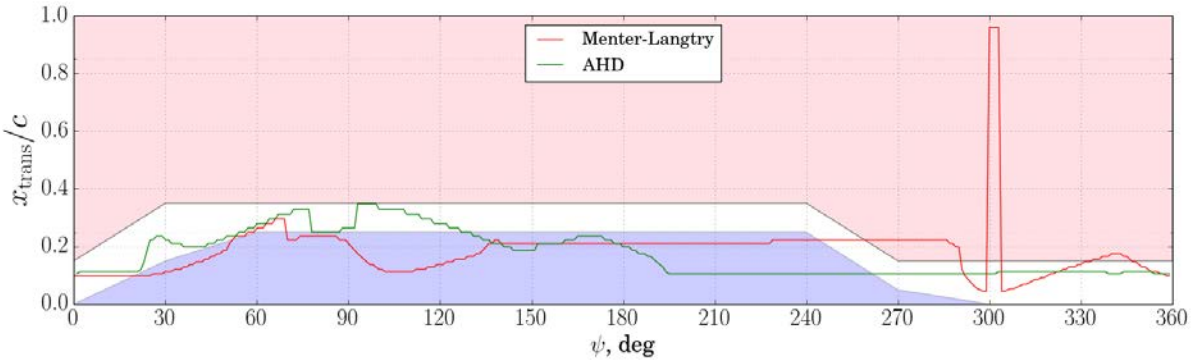

a) Upper side

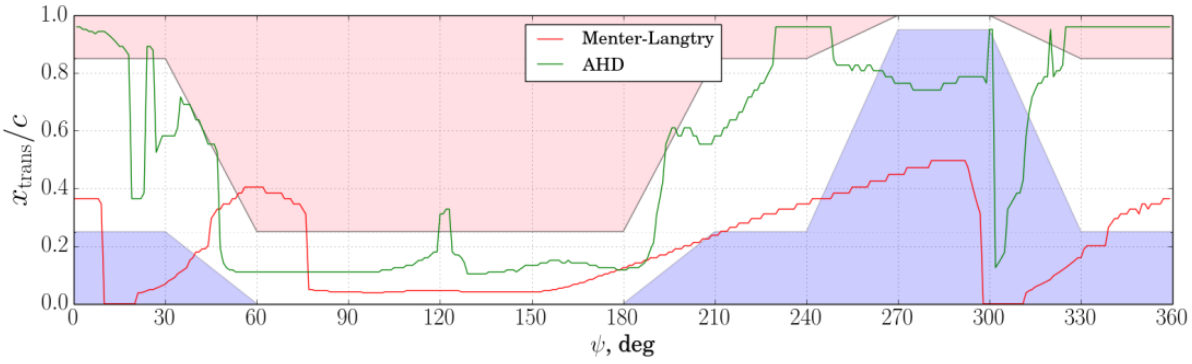

a) Lower side

Fig. 9. Azimuthal evolution of the transition location at section r/R=0.9 on the upper side (a) and lower side (b) of the rotor blade in forward flight: AHD criterion (green line), Menter-Langtry model (red line). Blue (respectively pink) region indicates laminar (respectively turbulent) region in the experiment.